Peer-reviewed version available at Materials 2019, 12, 1359; doi:10.3390/ma12081359

Pronounced impact of *p*-type carriers and reduction of bandgap in semiconducting ZnTe thin films by Cu doping for intermediate buffer layer in heterojunction solar cells

Waqar Mahmood [1,2,3,*],Saif Ullah Awan [4], Amad Ud Din [5], Sajid Butt [6], Andrew Thomas [2,7], A. Haq [8], Nazar Abbas Shah [3]

[1] Material Synthesis & Characterizations (MSC) Laboratory, Department of Physics, Fatima Jinnah Women University (FJWU), The Mall Rawalpindi-Pakistan.
[2] Photon Science Institute (PSI), School of Physics and Astronomy, University of Manchester, Oxford Road, M13 9PL Manchester-United Kingdom.
[3] Thin Films Technology (TFT) Research Laboratory, Department of Physics, COMSATS Institute of Information Technology (CIIT), Islamabad-Pakistan.
[4] Department of Electrical Engineering, NUST College of Electrical and Mechanical Engineering, National University of Science and Technology (NUST), Islamabad-Pakistan.
[5] Analog Electronics System (AES) Laboratory, Department of Physics, Fatima Jinnah Women University (FJWU), The Mall Rawalpindi-Pakistan.
[6] Department of Material Science & Engineering, Institute of Space Technology (IST), Islamabad-Pakistan.
[7] School of Materials, University of Manchester, Oxford Road, M13 9PL Manchester-United Kingdom.
[8] Department of Physics, Govt. Postgraduate College (Boys) Satellite Town, Rawalpindi-Pakistan.
*Corresponding author's Email: waqarmahmood@fjwu.edu.pk

Abstract

Stabilized un-doped Zinc Telluride (ZnTe) thin films were grown on glass substrates under vacuum using closed space sublimation (CSS) technique. A dilute copper nitrate solution (0.1/100 ml) was prepared for copper doping known as ion exchange process in the matrix of ZnTe thin film. The reproducible polycrystalline cubic structure of undoped and Cu doped ZnTe thin films with preferred orientation (111) was confirmed by X-rays diffraction (XRD) technique. Lattice parameter analyses verified the expansion of unit cell volume after incorporation of Cu species into ZnTe thin films samples. The micrographs of scanning electron microscopy (SEM) were used to measure the variation in crystal sizes of samples. The energy dispersive X-rays was used to validate the elemental composition of undoped and Cu-doped ZnTe thin films. The bandgap energy 2.24 eV of ZnTe thin film decreased after doping Cu to 2.20 eV may be due to the introduction of acceptors states near to valance band. Optical studies showed that refractive index was measured from 2.18 to 3.24 whereas thicknesses varied between 220 nm to 320 nm for un-doped and Cu doped ZnTe thin film respectively using Swanepoel model. The oxidation states of Zn^{+2}, Te^{+2} and Cu^{+1} through high resolution X-ray photoelectron spectroscopy (XPS) analyses was observed. The resistivity of thin films changed from ~10^7 Ω-cm for undoped ZnTe to ~1 Ω-cm for Cu-doped ZnTe thin film, whereas *p*-type

carrier concentration increased from $4 \times 10^{9}\ \mathrm{cm}^{-2}$ to $1.4 \times 10^{11}\ \mathrm{cm}^{-2}$ respectively. These results predicted that Cu-doped ZnTe thin film can be used as an ideal, efficient and stable intermediate layer between metallic and absorber back contact for the heterojunction thin film solar cell technology.

Keywords: Semiconductor thin films, CSS, ion-exchange, XRD, SEM, *p*-type carriers, band gap, solar cell

Introduction

CdTe based heterojunction tandem solar cells require a heavily doped, *p*-type back contact material of low resistivity as buffer layer capable of long term stability [1]. Simultaneously both high efficiency and stability of low cost photovoltaic cells are challenging issue in solar cell technology. Thin film of ZnTe was used as a stable back contact in CdTe based solar cell due to its small valence band offset between ZnTe and CdTe of 0.05 eV [2]. Among II-VI semiconductors, ZnTe semiconductor is naturally low carrier *p*-type system having direct band gap energy of 2.24 eV at room temperature, and an absorption coefficient of $10^{5}\ \mathrm{cm}^{-1}$ [3]. Thin films of ZnTe can absorb visible light without any phonon assisted mechanisms, it is an attractive choice for electro-optic and opto-electronic applications in the visible spectral range [3, 4]. ZnTe can play an ideal role as a stable and efficient intermediate layer with CdTe absorber and metallic back contact for heterojunction type solar cells technology. Experimentally, ZnTe semiconductor has proven itself as a low resistive, stable and efficient back contact for polycrystalline ZnTe/CdTe/CdS/ITO solar cells [5]. Previously, the values of electron affinity and work function of *p*-type CdTe thin film has been reported 4.28 eV and 5.78 eV respectively. Semiconductors readily form Schottky barrier with metals. However, an ohmic contact is highly desirable and the key issue in the fabrication of CdTe based photovoltaic cells [2]. Such high work function as mentioned above is not possible for metals as back contacts. Therefore, ZnTe is the best candidate to fulfill these requirements and compatibility with the CdTe based tandem solar cells [6]. High resistivity of ZnTe system is another bottleneck, therefore, a heavily doped *p*-type element is required to uplift the conductivity in ZnTe semiconductor [6, 7]. Copper (Cu) can act as a suitable *p*-type acceptor to achieve this goal. Also, due to the self-compensating effects of ZnTe semiconductor the *p*-type nature will remain same after Cu doping. Based on

previous studies, ZnTe is a potential candidate for solar cell application due to its ohmic contact with CdTe when doped with Cu.

Additionally, ZnTe semiconductors have found applications as cryogenic scintillators [8], opto-refractive, optical data processing [3, 4] blue LEDs [9], and now as a background buffer layer in second generation solar cells. The possibility of self-compensation doping [10, 11] by metallic dopants is one of the reasons for their extensive use in opto-electronics. Previously, ZnTe has been used in ternary compounds like MgZnTe, CdZnTe and HgZnTe as hybrid semiconductors [12]. ZnTe growth has been well documented by electro-chemical deposition, two-source evaporation, sputtering [12], and closed space sublimation (CSS) technique [13, 17]. The CSS technique is advantageous compared for competing coating methods to its smart utilization of materials, due to small substrate-source separations (5 mm). The physical properties of CSS deposited thin film can be enhanced by well controlled doping elements (e.g. Ag, Cu and In etc) through ion-exchange process [18]. The conductivity of the un-doped ZnTe system is *p*-type usually due to Zn vacancy defects (V_{Zn}) generation during thin film growth. The resistivity can be reduced by metal doping of group I with acceptor properties like Au, Li, Ag and Cu etc. Previous reports on Cu doped ZnTe reflects that it is a good dopant due to its shallow acceptor defect [2]. These defects are responsible for high carrier concentration that is usually enough to narrow down the ZnTe and metal interface barrier within tunneling regime. The Cu-doping probably increases the hole carrier concentration in ZnTe semiconductor, and therefore helps in the ohmic contact formation. Generally, if Cu replace Zn^{2+} species as Cu^{1+} state the probability of inducing *p*-type charge carriers will be greater as compared to Cu^{2+} state.

There are only a few reports on Cu–doped ZnTe thin films, and none on the oxidation state of Cu dopants. The search for novel materials in our group led us to report the development of a light Cu-doped ZnTe thin film samples. We have extended our research by studying ZnTe films doped with low concentrations of Cu. In current study, we report the optimized parameters for the synthesis of un-doped ZnTe thin film system with high hole concentration using CSS and ion-exchange method for Cu doping. We have studied the structural, morphology, elemental composition analysis, optical, electronic and electrical properties of un-doped and Cu-doped ZnTe thin film samples. The reduction of bandgap energy by introducing the shallow acceptor states while increases the hole carrier concentration of ZnTe thin film with Cu doping may be a

Peer-reviewed version available at Materials 2019, 12, 1359; doi:10.3390/ma12081359

good semiconducting material for intermediate buffer layer in heterojunction solar cells technology.

Experimental procedure:

Pure ZnTe powder (99.99 % of Aldrich chemicals) was used as source material using close spaced sublimation (CSS) technique to grow ZnTe thin films as shown in Fig. 1. The source material was kept in graphite boat whereas glass slides were used as a substrate with graphite slab for uniform heating on the top of glass slide. The source-substrate distance was optimized 5 mm for good quality of films. The temperature gradient was created by introduction of patterned mica sheet between source and substrate, as mica is thermal insulator. The halogen lamps of 1000 Watts (500 Watts) were used to heat source (substrate). K-type thermocouples with temperature controllers were inserted into graphite boat (slab) to monitor the temperatures of source (substrate). The roughing (rotary) pump was used to achieve a pressure of 10^{-2} mbar and latter employed diffusion pump to decrease it further down to 10^{-5} mbar. The halogen lamps were switched ON once the required level of vacuum was achieved and gradually increased the temperature up to 600°C (450°C) for source (substrate). The source lamp was switched OFF after the deposition time; $t_d = 300$ s for thin films was monitored by stop watch, whereas substrate lamp was kept switched ON for post-deposition annealing until source and substrate temperatures normalized. The chamber was left for cooling down to room temperature. A reddish brown ZnTe thin film was taken out from the chamber and tape test was done to check the film adherence. To obtain Cu-doped ZnTe thin film samples, un-doped ZnTe thin films were dipped in a low concentration copper nitrate $Cu(NO_3)_2$ solution in distilled water at (80 ± 5) °C. The doping was achieved and optimized by immersion time of 40 minutes and drying the samples after immersion. The optimized post annealing process was achieved on (350 ± 5) °C for 1 hour for the immersion of Cu in ZnTe structure.

The structural properties were recorded using PANanalytical spectrometer model X'PERT PRO. The XRD patterns were recorded with operating conditions of 40 keV, 30 mA with Cu-Kα line (λ=1.5406 Å). The scan speed was 1 s/step with 0.5° increments. X-ray beam scanned the sample at angle, θ from 20° to 60°. Scanning electron microscope (LSM-6490A analytical) was used to study the surface morphology at electron beam energies 15–20 keV with 8 nm resolution and EDX at 15 kV. The optical properties were calculated using spectrophotometer

of Perkin Elmer LAMDA 950 with UV Win lab software in ultraviolet, visible and near infrared (UV-Vis-NIR) regions. The electrical measurements were taken under magnetic field 0.5 T, current 1 nA at 300 K using Hall measurement system (HMS-5500 Ecopia). Cylindrical X-rays photoelectron spectroscopy (XPS) was adopted to investigate the bond strength and chemical oxidation states.

Results and Discussion:

X-Rays Diffraction (XRD):

X-rays diffraction (XRD) measurements were performed for un-doped ZnTe thin films and Cu-doped ZnTe thin films samples to study the crystal structure. The level of intensity for un-doped ZnTe thin films was much higher compared to that of a Cu-doped ZnTe thin film samples. The decrease in intensity of the Cu-doped samples is induced by stresses produced in ZnTe matrix due to Cu diffusion. The degradation in intensity of all diffracted peaks reflects that Cu is incorporated in ZnTe thin films. XRD data confirmed that (111) was the preferred orientation in ZnTe thin films and polycrystalline behavior with cubic phase confirmed by ICDD (reference no. 00-089-3054) as shown in Fig. 2. The peaks related to secondary phases or clustering issues of Cu-doped ZnTe system was not observed, which confirmed the presence of single system of polycrystalline nature. After Cu doping, the XRD peaks shifted toward lower angle (2θ) values as shown in the inset of Fig.2. The lattice parameters are calculated for cubic unit cell and are found 6.09 Å and 6.12 Å for un-doped and Cu-doped ZnTe thin film samples respectively. Overall, it is found that the unit cell volume increased as Cu incorporated into ZnTe thin films. As the atomic radius of Cu ~ 0.128 nm, which is larger than that of Zn ~ 0.074 nm [10], so it is predicted that after doping Cu the unit cell volume will be enhanced as we observed from XRD data. Crystallite sizes of un-doped and Cu-doped ZnTe thin film samples were calculated using Scherer's formula [10, 19], Eq. 1.

$$\text{Crystallite Size}(\text{C. S}) = \frac{0.9\lambda}{\beta \cos \theta} \quad (1)$$

Where 'λ' is the wavelength of X-rays, 'θ' is the angle of diffraction and 'β' is full width half maximum (FWHM). The crystallite size of un-doped ZnTe thin film was ~ 27 nm which was increased to ~ 50 nm after immersion and diffusion of Cu into ZnTe samples for 40 minutes.

Generally, cationic doping ions have tendency to incorporate as interstitial (occupy voids space) site or substitute cationic species in semiconductors. There is no metallic Cu peak or secondary phases has been observed and also the unit cell volume increased, so, it may suggest that Cu incorporates as substitutional sites. The possibility of Cu occupying at interstitial site is very low as the atomic size of Cu is larger than Zn species. Furthermore, we shall identify single phase of samples from Raman spectroscopy and the oxidation state of Cu from XPS measurements along with the conductivity type from Hall measurement.

Raman Spectroscopy:

A non-destructive Raman spectroscopy technique was used to check the crystal structure of ZnTe thin films at room temperature (RT). Transverse (TO) and longitudinal (LO) modes were checked in first order Raman spectra. The upper vibrational frequency is expressed by LO and lower frequency is denoted by TO mode [20]. RT-Raman spectroscopy measurements were performed and data of un-doped ZnTe thin films and Cu-doped ZnTe thin film samples has been presented in Fig. 3. The intensity of the Raman peaks decreased after incorporating Cu species into ZnTe thin film samples as compared to un-doped ZnTe thin films. These results are correlated with the XRD results showing degradation in the crystallinity of ZnTe thin film sample with doping effects of Cu.

In addition, RT-Raman spectra related to the TO and LO modes at the Γ-point, numerous two-phonon characteristics correlating to dissimilar signals in the ZnTe semiconductor are observed. Four vibrational Raman modes were observed at low frequency region 200 – 290 cm^{-1} for both samples. The pronounced peak at position 215, and two bands 238 and 245 are correspond to the vibration modes of multi-phonons L_O-ZnTe, $T_O(X)+T_A(X)$ and $L_O+T_A(L)$ respectively as calculated theoretically [20]. The Raman spectrum of both samples showed five multi-peaks under a large band in the range 290 - 400 cm^{-1}. The indication of each peak is very clear in the asymmetric band by kinks as shown in Fig. 3. According to the Raman vibrational mode selection rules of ZnTe [20], it was observed, the peak at position 300 and 313 corresponds to $2L_A$ (L) and $T_O(X)$ $+L_A(X)$ scattering modes. Similarly, $L_O(L)$ or $T_O(L)$ $+L_A(L)$ and $L_O(X)+T_O(X)$ are observed at positions 333 and 349 respectively in broad band as per selection rule system [20]. At the position 372 cm^{-1} a vibrational mode $2L_O(X)$ has been identified in these spectra. No peak or band was found beyond 500 cm^{-1} i.e. high frequency region. It is noticed, a

small shift towards lower frequency number of phonons was observed in the 1LO peak and 2LO peaks that may be due to disorder and strains introduced in ZnTe samples after Cu incorporation as reported in earlier studies [20-22].

Fig. 3 showed that the most prominent band of un-doped ZnTe thin films lie centered at 315 cm^{-1} contained different phonon modes was red-shifted to 313 cm^{-1} with incorporating Cu dopant in ZnTe thin film samples. This shift may be well corresponds to structural results, in the XRD data peaks are shifted towards lower angle, similarly Raman band and peaks are also shifted toward lower wave number after incorporating Cu into ZnTe matrix. Both the XRD and Raman characterizations, it may be suggested that the Cu dopant introduces substitutional defects at cationic site, which could be the responsible of generating higher stress in Cu-doped ZnTe thin film samples. So, eventually from XRD results, unit cell volume expands as Cu diffused into the ZnTe structure while the emission of phonon waves occurred at lower frequency number after Cu doping may strengthen the argument that Cu has properly replaced Zn species as substitutional defects. The lattice contraction has been observed by increasing the phonon frequency in case of ZnTe bulk crystal system [20, 21].

Furthermore, to better understand the effect of Cu doping in ZnTe thin film, It will be considered the concept of classical theory [21] given for LO and TO optical phonons by the following Eq. 2.

$$\omega LO \sim \omega TO \sim = (K/M_e)^{1/2} \quad (2)$$

where, K is force constant and M_e the extrinsic impurity atom's mass.

Case-1; if $M_e < M$ (mass of the parent atom), the vibrational frequency will be increased, such that $\omega_e > \omega$. However, in the case-2; if $M_e > M$ then $\omega_e < \omega$ and the frequency number of vibrational phonons will be reduced. Now in this case as the Cu substitute Zn species, but Zn species also remains within the interstitial sites of the stable cubic structure, so the mass of Cu-doped ZnTe thin film sample is greater than un-doped ZnTe thin film. So, using above equation approximation, case-2 is more relevant for this results. This is another mathematical reason that corresponds to experimental results that in Cu-doped ZnTe thin film samples the excited phonon frequency will be lower than the un-doped ZnTe sample as observed in RT-Raman spectra.

Microstructural Measurements:

Scanning electron microscopy (SEM) images of un-doped and Cu-doped ZnTe thin film samples have been demonstrated in Fig. 4 (a-b). It was observed, not proper circular but found elongated morphologies of crystals in both un-doped and Cu-doped ZnTe thin film samples. Due to higher agglomeration effects in un-doped ZnTe thin films, it is very difficult to measure the exact gain size of all grains; however we marked the crystals with their larger length only. In un-doped ZnTe thin films, the coalescence effect is more prominent and we observed lager sizes crystals as compared to Cu-doped ZnTe thin film samples. After incorporating Cu into ZnTe structure, the agglomeration effects reduced and the clarity of grains and grain boundaries are more visible and clear in Cu-doped ZnTe thin film samples as compared to un-doped ZnTe thin films. In Cu-doped ZnTe thin film samples, due to local stresses induced by diffusing Cu atoms into the ZnTe grains may be a reason for the separation of agglomerated grains. So, from microstructural data, we may overall argue, that Cu doping plays a vital role in the crystal for generating gain boundaries. Usually, larger size crystals show higher intensity, so un-doped ZnTe thin films showed higher intensity as it was observed from XRD data. A significant re-orientation and coalescence of the grains in other II-VI semiconductors are responsible for larger crystals sizes are reported previously [13, 18, and 23].

A tabulated result of EDX study was shown with Fig.4, emphasize the change in elemental composition of un-doped ZnTe thin films and Cu-doped ZnTe thin film samples. Cu concentration increased within ZnTe grains and therefore it is evident that Cu substitutes Te, hence Te content decreased, also it was redistributed whereas the concentration of Zn seemed to increase after Cu immersion in ZnTe thin film samples. The highest reported efficiency was 3 atomic % from 1 to 8 atomic % in J. Tang *et. al.* of Cu-doped ZnTe thin films [24].

Optical Transmission Spectroscopy:

Optical spectroscopy data in transmission mode of Cu-doped and un-doped ZnTe thin film samples were shown in Fig. 5. A decrease in transmission was observed in Cu-doped ZnTe thin film samples. The transmission of un-doped ZnTe thin films was 85 % which was decreased after Cu immersion down to 65 %. The band gap energy was calculated by absorption coefficient (α) as given in Eq. 3 and the relation for Tauc plot given by Eq. 4.

$$\frac{1}{d}\ln\left(\frac{1}{T}\right)\mathrm{h}\nu = \alpha \quad (3)$$

$$\alpha.\mathrm{h}\nu = A\left(\mathrm{h}\nu - E_g\right)^{N/2} \quad (4)$$

Where 'A' is a constant, '$\mathrm{h}\upsilon$'is photon energy, 'E_g' is energy band gap of material [25].

Un-doped ZnTe thin film has band gap of 2.24 eV, which was reduced to 2.20 eV, calculated through above relations, due to Cu incorporation as shown in inset of Fig.5. It was observed that the transmission and bandgap reduced for the Cu-doped in ZnTe thin film samples. The carrier concentration and grains of Cu-doped ZnTe thin film samples are responsible of band gap energy variation. The reduction of band gap energy indicates that defect levels were introduced after Cu immersion into ZnTe thin films. It is predicted that as the Cu^{+1} incorporates into Zn^{+2}, the possibility of hole carriers is obvious in Cu-doped ZnTe thin film samples. The Cu^{+1} dopant induces accepter states within bandgap, close to the valance band, so these acceptor states play a role for reducing the band gap energy in Cu-doped ZnTe thin film samples. The calculation of hole carrier concentration measurements will be correlated with these observed results. Similarly, variation of the band gap of un-doped ZnTe thin film was 2.24 eV reduced to 2.20 eV after Cu doping has been reported earlier [10] but this group did not identify the role of oxidation state of Cu species. A theoretical model of Swanpoel was used to calculate the optical thickness of thin films and refractive index by using the transmission data [26]. The refractive index $'n'$ can be calculated by the Eq. 5.

$$n = \frac{N+\sqrt{N^2-4s^2}}{2} \quad (5)$$

where N, the number of oscillations, is related to where maximum transmission (T_{max}) and minimum transmission (T_{min}) as,

$$N = 1 + s^2 + 4s \times \frac{T_{max}-T_{min}}{T_{max}\times T_{min}} \quad (6)$$

The thickness 'd' of the target thin films can be calculated using the Eq. 7 between wavelengths corresponding to maximum transmission (λ_{max}) and minimum transmission (λ_{min}).

$$d = \frac{\lambda_{max}\times\lambda_{min}}{4n(\lambda_{max}-\lambda_{\min})} \quad (7)$$

Optical parameters like refractive index varies from 2.18 to 3.24 and optical thickness ranging from 320 nm to 220nm were calculated using above equations (5-7) for un-doped and Cu-doped ZnTe thin film samples.

Peer-reviewed version available at Materials 2019, 12, 1359; doi:10.3390/ma12081359

X-ray Photoelectron Spectroscopy (XPS):

X-rays photoelectron spectroscopy (XPS) has been employed to study the electronic structure and chemical oxidation states of the ZnTe thin films species along the elemental information of Cu after doping. The binding energy (B.E.) of photoelectrons at 284.5 eV was used as a charge referencing standard for C-1s peak. CASA-XPS software was used to de-convolute the high resolution XPS peaks of Zn, Te and O species. Unfortunately, Cu signal was not captured during Cu-2p high resolution measurement may be due to very small amount of Cu doping concentration as confirmed by EDX. However, we identify Cu^{1+} peak in the high resolution Te-3d spectra as discussed below. The Lorentzian-Gaussian peaks were fitted on high resolution spectra of Zn, Te and O nicely. All the fitted graphs have non-linear Shirley type background and the other low-level elements were contained in baseline [17].

The survey scans of un-doped ZnTe and Cu-doped ZnTe thin film samples are presented in Fig. 6 (a-b). The orbital presence of the fundamental elements of these sample's zinc (Zn) and tellurium (Te) along oxygen (O) and carbon (C) has been observed. Cu peak was not observed in doped survey scan may be due to less percentage of doping. The signal of C-1s may be due to the presence of carbon tape used during XPS measurements. The presence of oxygen signal in survey scan may be due to the surface contamination with environmental oxygen. It is further studied, the high resolution XPS measurements of all compositions individually.

High resolution XPS of O-1s peaks of un-doped and Cu-doped ZnTe thin film sample has been demonstrated in Fig. 6 (c-d). The de-convoluted O-1s peak at 532.3eV and 535 eV in as deposited ZnTe thin films were examined. The peak at 532.3 was due to -OH contamination on the surface, it might be due to chemisorption or dissociated oxygen [27]. The peak at 535 eV was the indication of O-C species. The de-convoluted peak positions for O-1s after Cu doping in ZnTe thin films were observed at 531.50 eV, 533.6 eV and 538.3eV [28]. The peak at 531.5 eV was due to concentration variation in oxygen vacancies of deficient region. The chemisorption or OH species or dissociated oxygen was attributed at the peak of 533.6 eV and the peak located at 538.3 eV might be due to the O-C contamination. The carbon or oxygen on the surface treated as contamination are the existence of auxiliary oxides formation. The level of intensities relates to the strong bonding between the species [17].

The high resolution XPS measurements were performed for Zn-2p spectra, while the de-convoluted fitted peaks for Zn-$2p_{3/2}$ and Zn-$2p_{1/2}$ of un-doped and Cu-doped ZnTe thin film samples are shown in Fig.7 (a-b) respectively. The intensity of Zn-$2p_{3/2}$ peaks is usually higher however the binding energy (B.E) is less than Zn-$2p_{1/2}$ [22]. These fitted Zn-$2p_{3/2}$ peaks of un-doped ZnTe thin films were observed at 1024.48 (due to Zn^{2+} oxidation) and 1023.63 eV (Zn metallic) while $2p_{1/2}$ lies at 1048.30 eV (due to Zn^{+2} oxidation) and 1046.84 eV (Zn metallic) peak central positions. The spin orbit coupling (ΔE = Zn-$2p_{1/2}$- Zn-$2p_{3/2}$ = 23.82 eV) for un-doped ZnTe sample showing Zn^{2+} oxidation state is calculated. It is observed that in un-doped ZnTe thin films the 100 % Zn-ions are not bonded with Te-ions. After doping of Cu in ZnTe matrix, the high resolution XPS Zn-2p peaks were shifter towards higher order values mostly due to doping effects [12]. The higher intensity de-convoluted Zn-$2p_{3/2}$ peak at position 1030.49 eV and Zn-$2p_{1/2}$ at 1053.61 eV were obtained after fitting with ΔE = 23.12 eV that is showing Zn^{2+} state. For Cu-doped ZnTe thin film samples the calculated Zn-$2p_{3/2}$ peak at position 1023.86 eV and Zn-$2p_{1/2}$ at eV 1047.16 are related to un-bounded Zn species. The results may be inferred that with Cu doping, we observed less amount of Zn in metallic form as compared to Zn^{2+} state. In other words, Cu supports the introduction of more Zn^{2+} states in Cu-doped ZnTe thin film samples as compared to un-doped ZnTe thin film.

High resolution XPS spectra after devolution of Te-3d for un-doped and Cu-doped samples have been presented in Fig.7 (c-d). The peak positions at 587.11 eV, 575.93 eV and 572.31 eV were observed for un-doped ZnTe thin films whereas after Cu immersion the peaks were located at 593.55 eV, 589.69 eV, 586.74 eV, 579.17 eV, 576.50 eV and 572.10 eV. The prominent, de-convoluted Te-$3d_{5/2}$ and $3d_{3/2}$ peaks at positions (i.e. 587.46 and 576.96 for un-doped and for Cu doped 586.96 and 576.86) are observed, these are mostly due to oxide tellurium (TeO_2, TeO_3) as reported previously. Usually in ZnTe system, the bonding between Te-Zn exist and can be observed during high resolution XPS spectra of Te-3d [7]. It is found Te-$3d_{3/2}$ at peak position 572.73eV for both samples while we noticed Te-$3d_{5/2}$ at peak position 583.16 eV for only Cu-doped ZnTe thin film sample. However, in literature mostly 4 peaks are observed in Te-3d spectra while the observation is different for Te-3d of our un-doped and doped sample [2]. In un-doped ZnTe thin film, the XPS spectra peak of Te-$3d_{5/2}$ is not present, which may indicate that less amount of Zn spices are bonded with Te in the absence of Cu doping. So, here Cu plays a major role for enhancing the numbers of bonds between Te-Zn species. It is observed, Auger

peaks due to the incorporation of Cu into the matrix of ZnTe thin films, another prominent peak at 569.87 eV were notices and corresponds to Cu^{+1} species as reported in literature [29, 30]. Similarly, we found Zn *LMM* Auger peak [31] at position 579.60 eV in Cu-doped ZnTe thin film samples. These two Auger peaks were found only in Cu-doped sample and did not observed any indication of these signals in un-doped ZnTe thin films.

Overall, an interesting result was obtained from the electronic properties of both samples and there is clear indication that Cu^{+1} has been incorporated into the matrix of ZnTe systems. There is no signal of Cu^{+2} has been observed in the XPS measurements. In this study, and the observed results from XPS data the Cu^{+1} will induce larger number of hole carriers in ZnTe thin film systems. For further verification of Cu^{1+}, electrical measurements using Hall setup performed to quantify the hole carrier concentration as discussed below. In our current study the electron transport of ZnTe thin films doped with Cu have been observed with the identification of the oxidation state of Cu as Cu^{1+} while earlier study did not focus on the oxidation state of Cu (i.e. Cu^{1+} or Cu^{2+}) [12].

Electrical Properties:

Vander pauw technique [32] was employed to calculate the electron transport of Cu-doped and un-doped ZnTe thin film samples. The electrical reading was carried out five times at room temperature to ascertain them and minimize the errors. Un-doped ZnTe thin film possesses resistivity of the order of mega ohm-cm which was reduced up to 1 ohm-cm after Cu immersion in matrix of ZnTe thin films. The Cu doping resulted in the reduction of resistivity due to increase in charge carriers in ZnTe thin film. The resistivity of un-doped ZnTe thin film was ˜ 10^7 Ω-cm that was reported by A. Maqsood *et. al.* [33] decreased to ~ 0.5 Ω-cm after 40 min Cu diffusion into ZnTe sample with concentrated solution. The mobility of un-doped ZnTe thin film was 16 cm^2/Vs and increased to ~ 350 cm^2/Vs for Cu immersed ZnTe thin film samples. The mobility increased after Cu-doping was due to the increase in the carrier concentration. The calculated sheet concentration for un-doped ZnTe thin film of ~ $4 \times 10^9/cm^2$ increased by two orders of magnitude to $1.4 \times 10^{11}/cm^2$ for 40 min Cu-doped ZnTe thin film samples. We observed the *p*-type conductivity in these Cu-doped ZnTe thin film samples. The substitution of Zn^{+2} by Cu^{+1} in doped samples can be obvious as the hole carrier concentration increased in

Peer-reviewed version available at Materials 2019, 12, 1359; doi:10.3390/ma12081359

doped samples. These electrical results also support to the chemical results were measured by XPS and bandgap reduction in transmission measurements.

Discussion and Conclusions:

CdTe based solar cells are potential candidate for large scale fabrication, however low resistive back contact with p-type CdTe still under attention. Mott-Schottky theory limits CdTe Fermi level pinning up to certain extent. The acceptor compensation in CdTe with limiting effectiveness of contact and low doping efficiency that rely the quantum tunneling [34]. These constraints for forming good ohmic contact of CdTe like Au, Ag or Cu. The intermediate layer should enable high p-type doping and small valence band offset with CdTe to get low resistance quantum mechanical tunneling. ZnTe is supposed to be good candidate for such intermediate layer. The small valence band offset for CdTe/ZnTe with Cu doping was introduced to $> 10^{18} cm^{-3}$ but the identification of Cu^{+1} or Cu^{+2} is not clear over there. The ZnTe contacts got reasonable success and stability after Cu immersion in solar cell devices. Cu is a quick diffuser in many materials [12]. Cu contents in semiconducting material were related to different instabilities in CdTe based solar cells. But we focus on the investigation of Cu^{+1} diffusion into the matrix of ZnTe thin film system at optimized parameters with reproducing the same carrier concentration repeatedly.

Thin films of ZnTe were synthesized at optimized parameters by sublimated through CSS technique and Cu doping in ZnTe thin films was achieved using ion exchange process. These samples showed polycrystalline nature with (111) direction as a preferred orientation. The structural and morphological study correlated, as crystallite size increases result in the increase of grains of Cu-doped ZnTe thin film samples [13]. The elemental composition confirmed the Cu contents in ZnTe thin films using EDX. The transmission decreased from 85 % to 65 % after Cu immersion in optical properties. A slight decrease in band gap energy was observed after Cu immersion in ZnTe thin film samples. The resistivity decreased several order of magnitude (10^6 to 1 Ω-cm) after Cu doping in electrical measurements. After doping Cu into the matrix of ZnTe, the unit cell volume increase as the ionic size of Cu species are larger than Zn species. The unit cell volume expansion may be related to the reduction of bandgap. From the Hall measurements, the resistivity reduces of the ZnTe bare thin film as compared to Cu doped sample as hole carrier increased due to the charge difference between Cu^{+1} and Zn^{+2} species. These p-type charge

carriers can play a vital role for the reduction of bandgap energy after incorporating Cu into ZnTe with the introduction of accepter states defects near to valance band. These defects states are also identified from high resolution XPS studies of these samples. The XRD data confirmed the homogeneous distribution of Cu in ZnTe thin film samples. Unit cell volume increased confirmed the substitutional doping of Cu in crystal structure of ZnTe. While, the XPS measurement confirmed the presence of Cu^{+1} oxidation state in ZnTe sample. These results support the picture and are correlated with electric measurements. Cu^{+1} has confirmed the substitution of Zn^{+2} species, so the charge carrier's concentration of *p*-type should be enhanced obviously as we found in electrical properties. So, at this stage our doped sample showed p-type conductivity in Cu^{+1} doped ZnTe thin film samples. The decreasing trend in resistivity of Cu-doped ZnTe thin film samples showed the semiconducting behavior.

Acknowledgements:

The authors are thankful to Higher Education Commission (HEC), Pakistan for providing necessary fund through project # 20-1187/R&D/09 and International Research Support Initiative Program (IRSIP) of HEC through pin # IRSIP 23 Ps 15.

Bibliography:

1. Ho, S. M. *et. al.* Zinc Telluride Thin Films: A Review. *Asian J. Chem.* **30 (3)** 469-473 (2018).
2. Wang, W., Xia, G., Zheng, J., Feng, L. & Hao, R. Study of polycrystalline ZnTe (ZnTe:Cu) thin films for photovoltaic cells. *J. Mater. Sci. Mater. Electron.* **18,** 427–431 (2007).
3. Ahamed, J. U., Begum, N. P. & Khan, M. N. I. Property elucidation of vacuum-evaporated zinc telluride thin film towards optoelectronic devices. *Sadhana - Acad. Proc. Eng. Sci.* **42,** 1773–1781 (2017).
4. Fields, J. D. *et al.* Printed interconnects for photovoltaic modules. *Sol. Energy Mater. Sol. Cells* **159,** 536–545 (2017).
5. Gessert, T. A. & Coutts, T. J. Development and analysis of Cu-doped ZnTe for use as a back contact interface for CdS/CdTe solar cells. in *AIP Conference Proceedings* **306,** 345–353 (1994).
6. Gessert, T. A. *et al.* II-VI Material Integration With Silicon for Detector and PV Applications. *MRS Adv.* **1,** 3391–3402 (2016).
7. Potlog, T., Duca, D. & Dobromir, M. Temperature-dependent growth and XPS of Ag-doped ZnTe thin films deposited by close space sublimation method. *Appl. Surf. Sci.* **352,** 33–37 (2015).
8. Mikhailik, V. B. *et al.* ZnTe cryogenic scintillator. *J. Lumin.* **188,** 600–603 (2017).
9. Hou, L. *et al.* Interfacial fabrication of single-crystalline ZnTe nanorods with high blue

fluorescence. *J. Am. Chem. Soc.* **135,** 10618–10621 (2013).
10. Tariq, G. H., Niaz, N. A. & Anis-Ur-Rehman, M. Effects of dopants profile on physical properties of ZnTe thin films. *Chalcogenide Lett.* **11,** 461–470 (2014).
11. Shaaban, E. R., Kansal, I., Mohamed, S. H. & Ferreira, J. M. F. Microstructural parameters and optical constants of ZnTe thin films with various thicknesses. *Phys. B Condens. Matter* **404,** 3571–3576 (2009).
12. El Akkad, F. & Abdulraheem, Y. Morphology, electrical, and optical properties of heavily doped ZnTe:Cu thin films. *J. Appl. Phys.* **114,** 183501 (2013).
13. Mahmood, W. & Shah, N. A. CdZnS thin films sublimated by closed space using mechanical mixing: A new approach. in *Optical Materials* **36,** 1449–1453 (2014).
14. Abken, A. E., Halliday, D. P. & Durose, K. Photoluminescence study of polycrystalline photovoltaic CdS thin film layers grown by close-spaced sublimation and chemical bath deposition. *J. Appl. Phys.* **105,** 64515 (2009).
15. Mahmood, W. *et al.* Investigation of substrate temperature effects on physical properties of ZnTe thin films by close spaced sublimation technique. *Chalcogenide Lett.* **10,** 273–281 (2013).
16. Mahmood, W., Ali, J., Zahid, I., Thomas, A. & ul Haq, A. Optical and electrical studies of CdS thin films with thickness variation. *Optik (Stuttg).* **158,** 1558–1566 (2018).
17. Mahmood, W., Thomas, A., Haq, A. ul, Shah, N. A. & Nasir, M. F. Reduced electrical performance of Zn enriched ZnTe nanoinclusion semiconductors thin films for buffer layer in solar cells. *J. Phys. D. Appl. Phys.* **50,** 255503 (2017).
18. Mahmood, W. & Shah, N. A. Effects of metal doping on the physical properties of ZnTe thin films. *Curr. Appl. Phys.* **14,** 282–286 (2014).
19. Mahmood, W. *et al.* Role of Ag^{1+} substitutional defects on the electronic and optical properties of *n*-type CdS thin films semiconductor for sustainable and stable window layer in solar cells technology. *Optical Materials* **85** 143-152 (2018).
20. Irwin, J. C. & LaCombe, J. Raman Scattering in ZnTe. *J. Appl. Phys.* **41,** 1444–1450 (1970).
21. Cao, L. Z. *et al.* Influence of stress on Raman spectra in Ba 1− x Sr x TiO 3 thin films. *J. Phys. D. Appl. Phys.* **39,** 2819–2823 (2006).
22. Amirtharaj, P. M. & Pollak, F. H. Raman scattering study of the properties and removal of excess Te on CdTe surfaces. *Appl. Phys. Lett.* **45,** 789–791 (1984).
23. Shah, N. A. & Mahmood, W. Physical properties of sublimated zinc telluride thin films for solar cell applications. *Thin Solid Films* **544,** 307–312 (2013).
24. Tang, J., Mao, D. & Trefny, J. U. Effect of Cu doping on the properties of ZnTe:Cu thin films and CdS/CdTe/ZnTe solar cells. in *AIP Conference Proceedings* **394,** 639–646 (AIP, 1997).
25. Siddiqui, G., Ali, J., Doh, Y.-H. & Choi, K. H. Fabrication of zinc stannate based all-printed resistive switching device. *Mater. Lett.* **166,** 311–316 (2016).
26. Swanepoel, R. & Swanepoel, R. Determination of the thickness and optical constants of amorphous silicon. *J. Phys. E.* **16,** 1214–1222 (1983).
27. Ullah Awan, S., Hasanain, S. K., Bertino, M. F. & Hassnain Jaffari, G. Ferromagnetism in Li doped ZnO nanoparticles: The role of interstitial Li. *J. Appl. Phys.* **112,** 103924 (2012).
28. Awan, S. U., Hasanain, S. K., Bertino, M. F. & Jaffari, G. H. Effects of substitutional Li on the ferromagnetic response of Li co-doped ZnO:Co nanoparticles. *J. Phys. Condens. Matter* **25,** 156005 (2013).
29. Dabera, G. D. M. R. *et al.* Retarding oxidation of copper nanoparticles without electrical

isolation and the size dependence of work function. *Nat. Commun.* **8,** 1894 (2017).

30. Kozak, D. S., Sergiienko, R. A., Shibata, E., Iizuka, A. & Nakamura, T. Non-electrolytic synthesis of copper oxide/carbon nanocomposite by surface plasma in super-dehydrated ethanol. *Sci. Rep.* **6,** 21178 (2016).
31. Awan, S. U. *et al.* Study of room temperature Raman scattering and XPS, high temperature electrical and low temperature magnetic properties of Zn 1− y Li y O (0.00 ≤ y ≤ 0.10) nanoparticles. *Smart Mater. Struct.* **24,** 115025 (2015).
32. Mahmood, W. Fabrication and Characterization of II-VI Semiconductor Thin Films and the Study of Post Doping Effects. *Higher Education Commission, Pakistan* 1–135 (2015). Available at: http://eprints.hec.gov.pk/id/eprint/6358.
33. Aqili, A. K. S., Maqsood, A. & Ali, Z. Properties of copper-doped ZnTe thin films by immersion in Cu solution. *Appl. Surf. Sci.* **180,** 73–80 (2001).
34. Teeter, G. X-ray and ultraviolet photoelectron spectroscopy measurements of Cu-doped CdTe(111)-B: Observation of temperature-reversible CuxTe precipitation and effect on ionization potential. *J. Appl. Phys.* **102,** 34504 (2007).

Table of Figures

Peer-reviewed version available at Materials 2019, 12, 1359; doi:10.3390/ma12081359

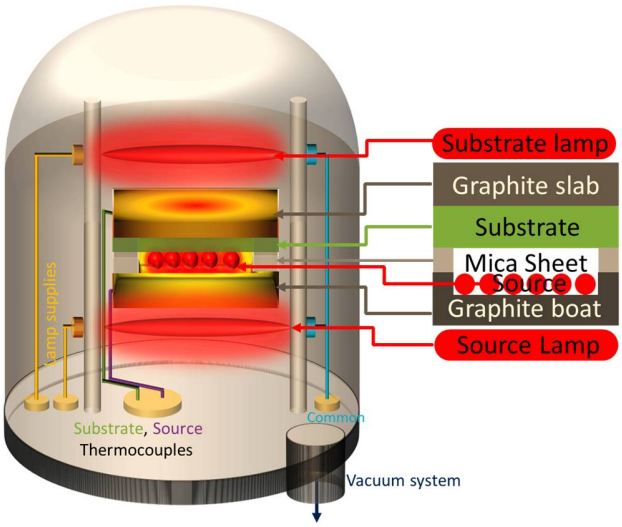

Figure 1: Schematic of Close Spaced Sublimation (CSS) technique used for deposition of ZnTe thin films

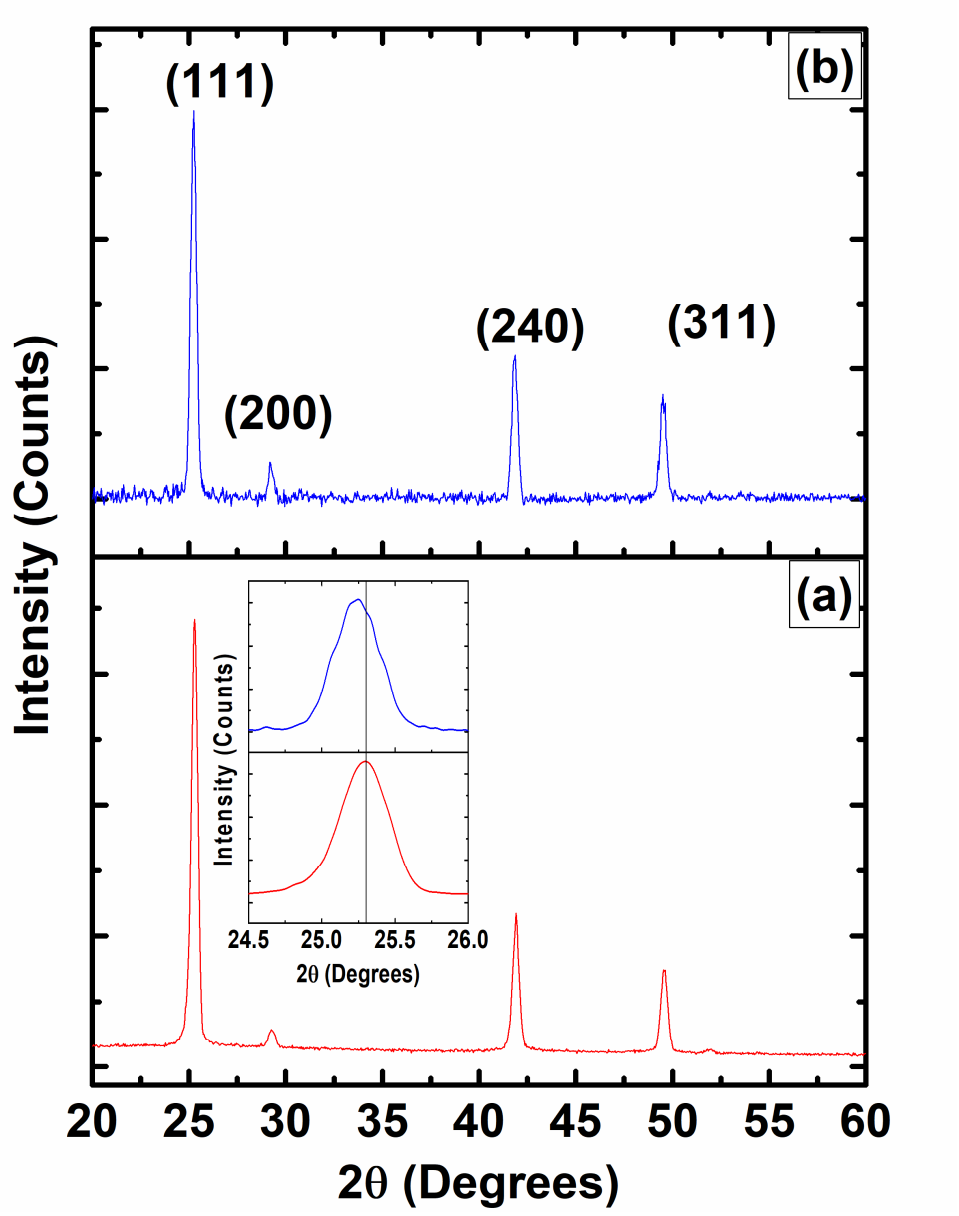

Figure 2: X-rays diffraction patterns of (a) un-doped ZnTe thin film and (b) Cu-doped ZnTe thin film samples. Inset shows the post-doping shift in (111) peak

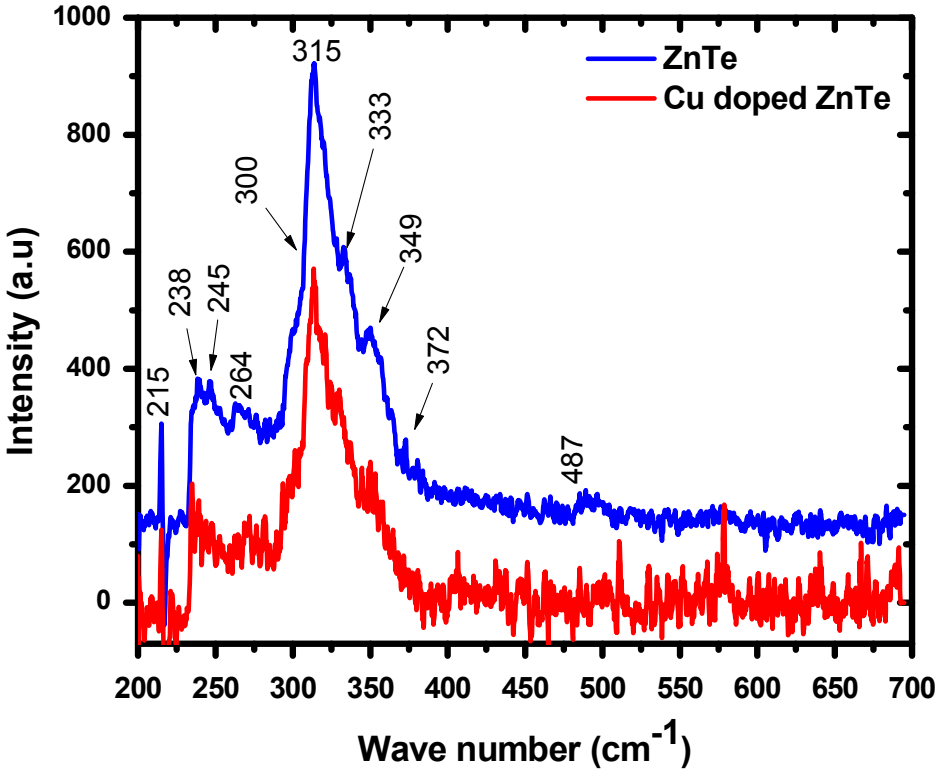

Figure 3: Room temperature Raman spectra of un-doped ZnTe and Cu-doped ZnTe thin film samples

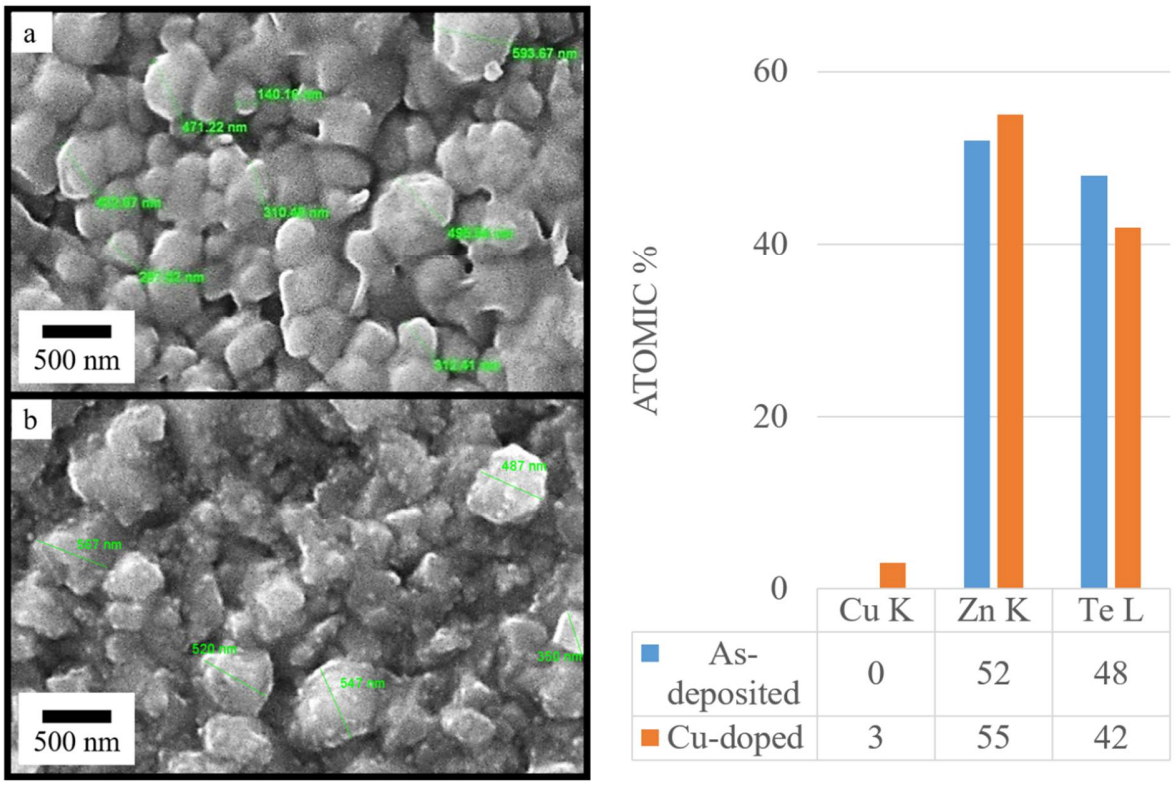

Figure 4: Scanning Electron Micrographs of a) un-doped and b) Cu-doped ZnTe thin film samples with EDX analyses of un-doped and Cu-doped ZnTe thin film samples shows a Cu content of 3 atomic % in Cu-doped samples

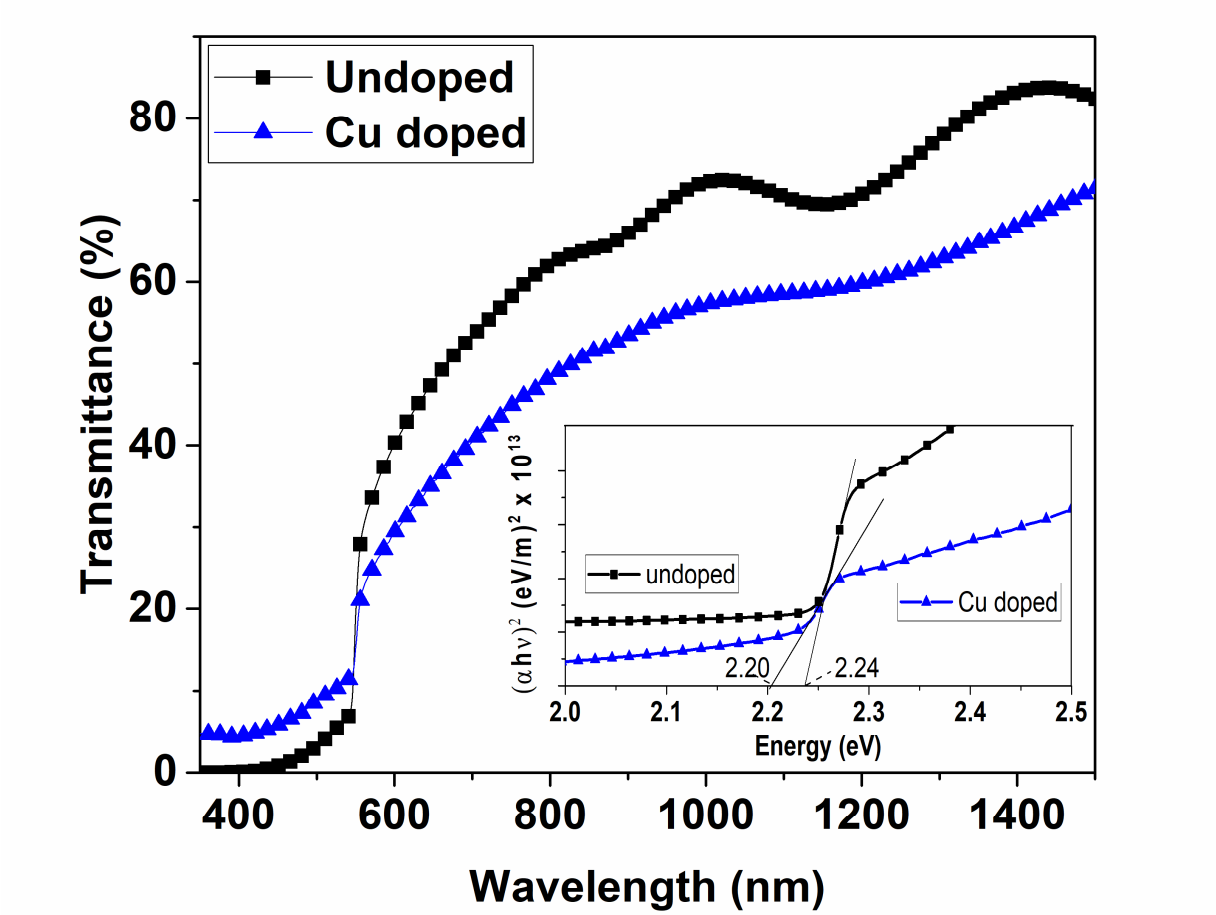

Figure 5: Transmission spectra of un-doped ZnTe thin films and Cu-doped ZnTe samples, the inset shows the calculation of bandgaps, using Tauc plots

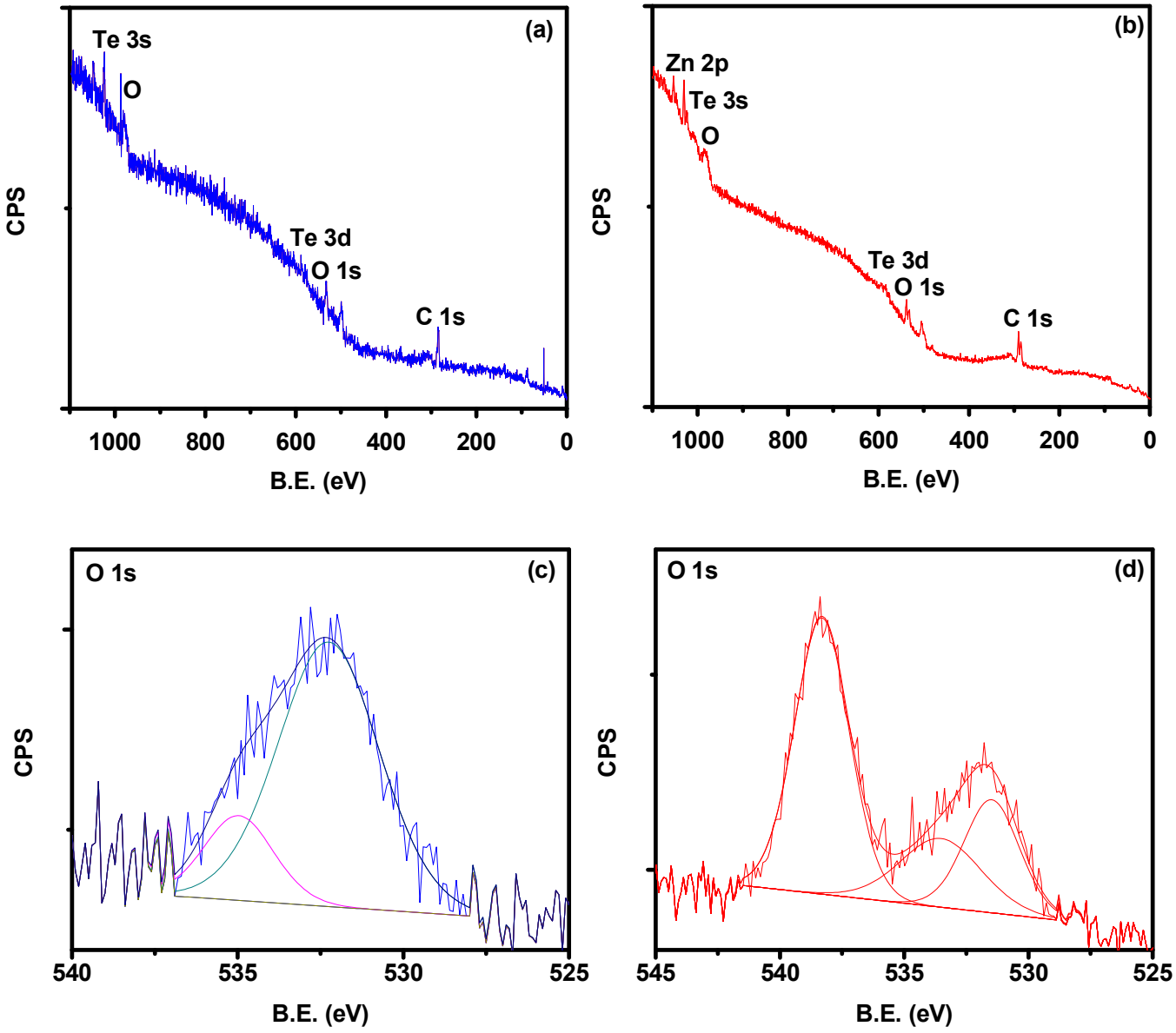

Figure 6: XPS Survey scan of (a) un-doped and (b) Cu-doped ZnTe thin film samples. De-convoluted XPS analysis of Oxygen-1s for (c) un-doped and (d) Cu-doped ZnTe thin film samples

Peer-reviewed version available at Materials 2019, 12, 1359; doi:10.3390/ma12081359

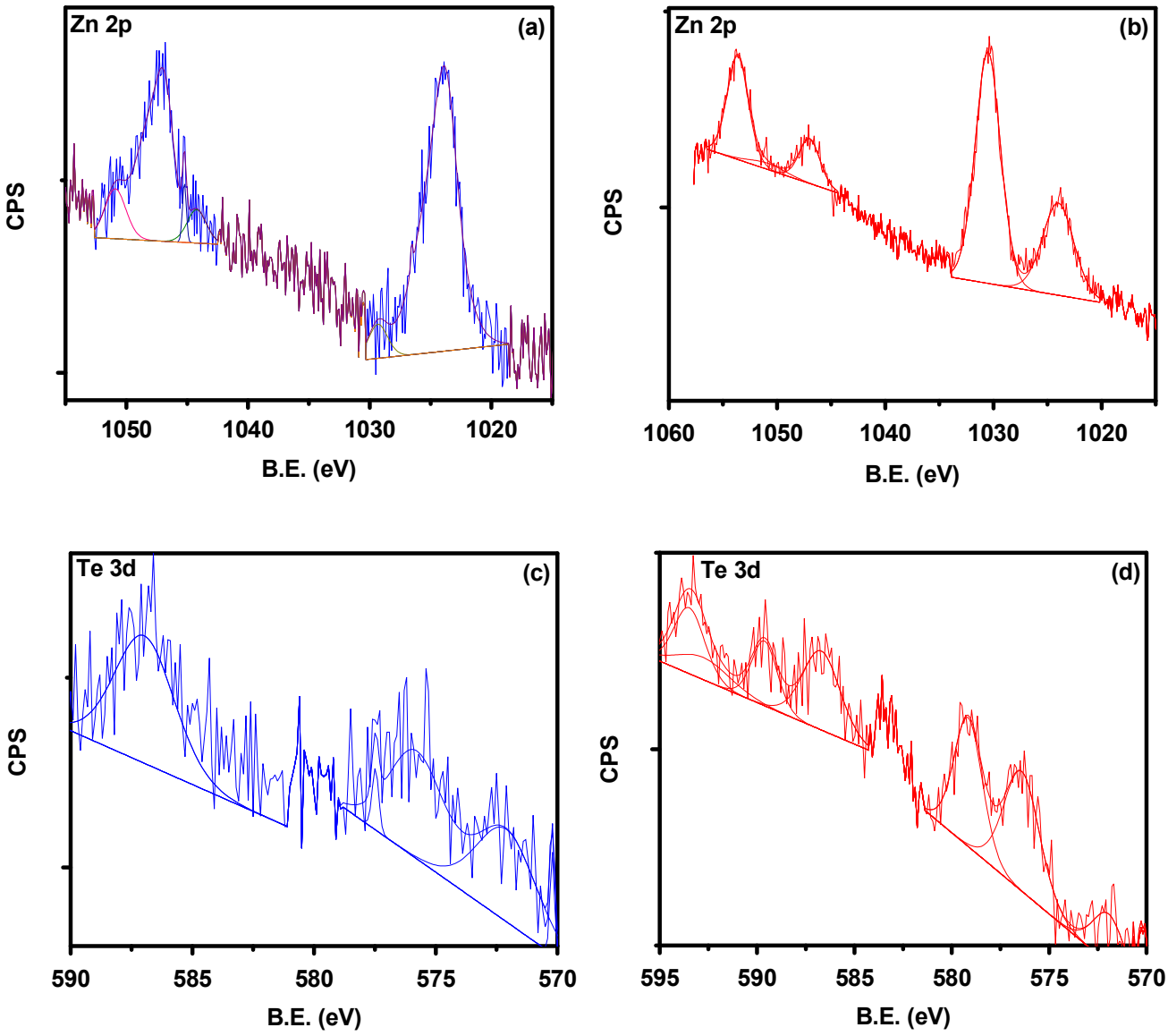

Figure 7: De-convoluted XPS analysis of Zinc-2p for (a) un-doped and (b) Cu-doped ZnTe thin film samples. De-convoluted XPS analysis of Tellurium-3d for (c) un-doped and (d) Cu-doped ZnTe thin film samples